Available online at www.sciencedirect.com

SciVerse ScienceDirect

Proceedings of the Combustion Institute 34 (2013) 565–571

Proceedings of the Combustion Institute

www.elsevier.com/locate/proci

On the rate constants of $OH + HO_2$ and $HO_2 + HO_2$: A comprehensive study of H_2O_2 thermal decomposition using multi-species laser absorption

Zekai Hong [1], King-Yiu Lam, Ritobrata Sur, Shengkai Wang, David F. Davidson *, Ronald K. Hanson

Department of Mechanical Engineering, Stanford University, Stanford, CA 94305, USA

Available online 19 July 2012

Abstract

Hydrogen peroxide (H_2O_2) and hydroperoxy (HO_2) reactions present in the H_2O_2 thermal decomposition system are important in combustion kinetics. H_2O_2 thermal decomposition has been studied behind reflected shock waves using H_2O and OH diagnostics in previous studies (Hong et al. (2009) [9] and Hong et al. (2010) [6,8]) to determine the rate constants of two major reactions: $H_2O_2 + M \rightarrow 2OH + M$ (k_1) and $OH + H_2O_2 \rightarrow H_2O + HO_2$ (k_2). With the addition of a third diagnostic for HO_2 at 227 nm, the H_2O_2 thermal decomposition system can be comprehensively characterized for the first time. Specifically, the rate constants of two remaining major reactions in the system, $OH + HO_2 \rightarrow H_2O + O_2$ (k_3) and $HO_2 + HO_2 \rightarrow H_2O_2 + O_2$ (k_4) can be determined with high-fidelity.

No strong temperature dependency was found between 1072 and 1283 K for the rate constant of $OH + HO_2 \rightarrow H_2O + O_2$, which can be expressed by the combination of two Arrhenius forms: $k_3 = 7.0 \times 10^{12}\exp(550/T) + 4.5 \times 10^{14}\exp(-5500/T)$ [$cm^3\,mol^{-1}\,s^{-1}$]. The rate constants of reaction $HO_2 + HO_2 \rightarrow H_2O_2 + O_2$ determined agree very well with those reported by Kappel et al. (2002) [5]; the recommendation therefore remains unchanged: $k_4 = 1.0 \times 10^{14}\exp(-5556/T) + 1.9 \times 10^{11+}\exp(709/T)$ [$cm^3\,mol^{-1}\,s^{-1}$]. All the tests were performed near 1.7 atm.

1. Introduction

Despite its simplicity, the H_2O_2 thermal decomposition system features some of the most important elementary reactions for describing combustion kinetics, particularly reactions involving perhydroxyl radical. Although the system can be described by only a handful of reactions

$$H_2O_2 + M \rightarrow 2OH + M \quad (1)$$

$$OH + H_2O_2 \rightarrow H_2O + HO_2 \quad (2)$$

$$OH + HO_2 \rightarrow H_2O + O_2 \quad (3)$$

$$HO_2 + HO_2 \rightarrow H_2O_2 + O_2 \quad (4)$$

$$OH + OH \rightarrow H_2O + O \quad (5)$$

* Corresponding author.
E-mail address: dfd@stanford.edu (D.F. Davidson).
[1] Currently at General Electric Company Global Research Center, Niskayuna, NY 12309, USA.

1540-7489/$ - see front matter © 2012 The Combustion Institute. Published by Elsevier Inc. All rights reserved.
http://dx.doi.org/10.1016/j.proci.2012.06.108

and just four hydrogen-containing species (H_2O_2, H_2O, OH, HO_2), these reactions and species are not well characterized. As well, the UV absorption cross-sections of HO_2 and H_2O_2 at temperatures above 1000 K were only measured by one group more than 20 years ago and their values are, to some degree, tied to kinetic interpretation [1–3].

In addition to the uncertainty in the HO_2 and H_2O_2 absorption cross-section data, the rate constants of some of these aforementioned reactions are still subject to large uncertainties. For example, the studies by Hippler et al. [4] and Kappel et al. [5] suggest a strong temperature dependence of the rate constant of Reaction (3) (k_3) with a narrow rate constant minimum near 1250 K or 1000 K, respectively. In contrast, recent studies by Hong et al. [6] and Srinivasan et al. [7] show no evidence of such strong temperature dependence of k_3 near 1000 K. However, results reported by Hong et al. [6] were obtained at temperatures higher than 1600 K, which could not directly resolve the possible discrepancy near 1000 K. Furthermore, Reaction (3) was only of secondary importance in the reacting system investigated by Srinivasan et al. [7]; hence scatter in the inferred k_3 values prohibit a definite conclusion regarding k_3 temperature dependency near 1000 K.

Similar to k_3, the rate constant k_4 of Reaction (4), $HO_2 + HO_2 \rightarrow H_2O_2 + O_2$, may require a re-evaluation, as most available experimental data at combustion temperatures were obtained by studying the H_2O_2 thermal decomposition system [1,3,5], with the exception of one study [3] that also investigated $(CH_3O)_2/O_2$ mixtures. In a closely correlated reacting system such as the H_2O_2 thermal decomposition system, once k_3 can be determined with better accuracy, an improved understanding of k_4 naturally follows. In addition, recent updates in the rate constants of Reactions (1), (2), and (5) [8,9,11] can help to reduce the uncertainty in the re-evaluated k_4 values.

Recent advances in laser diagnostics [10] have, for the first time, paved the way to gain comprehensive understanding of the H_2O_2 thermal decomposition system by experimentation. In 2010, Hong et al. [9] introduced a sensitive H_2O diagnostic based on tunable diode laser absorption near 2.5 μm to study H_2O_2 thermal decomposition behind reflected shock waves. Shortly afterwards, an OH absorption diagnostic near 308 nm was combined with the H_2O diagnostic to investigate H_2O_2 pyrolysis in a shock tube [8]. As there are only four hydrogenous species in the reacting system, a diagnostic for a third hydrogen-containing species, HO_2, together with conservation of hydrogen, should completely determine the system. Therefore, the goal of the current work is to perform a comprehensive study of H_2O_2 pyrolysis by measuring the time-histories of H_2O, OH, and HO_2 species simultaneously.

2. Experimental setup

H_2O_2 thermal decomposition experiments were performed in a shock tube behind reflected shock waves. The stainless-steel shock tube consists of a 3.7 m driver section and a 10 m driven section, both of which have an inner diameter of 15.2 cm. Temperatures and pressures in the post-shock region were determined from the incident shock speed at the endwall using standard normal shock relations. The incident shock speed was measured using a series of piezoelectric pressure transducers over the last 1.5 m of the shock tube and linearly extrapolated to the endwall. The shock tube was equipped with a turbo-molecular pump that is capable of obtaining an ultimate pressure below 10^{-6} torr, with a leak and outgassing rate of $\sim 3 \times 10^{-6}$ torr/min.

Laser diagnostics for three species (H_2O, OH, and HO_2) were simultaneously used to study H_2O_2 decomposition behind reflected shock waves. All three laser beams were passed across the diameter of the shock tube at a location 2 cm from the shock tube endwall and were in the same axial plane for easy synchronization.

H_2O and OH time-histories were measured using a tunable diode laser near 2.5 μm and a ring-dye laser near 308 nm, respectively. These two diagnostics have been successfully utilized in previous H_2O_2 pyrolysis studies [6,8,9]; only brief descriptions are provided in this paper. A distributed feedback (DFB) diode laser from Nanoplus GmbH was used to access a strong H_2O absorption transition at 2550.96 nm (3920.09 cm^{-1}) within the H_2O v_3 fundamental vibrational band. The transmitted laser intensity after H_2O absorption was detected by a liquid nitrogen-cooled InSb detector. For the OH diagnostic, the $R_1(5)$ line of the $A^2\Sigma^+ - X^2\Pi$ (0,0) band near 306.7 nm was chosen. 1–2 mW of UV light at 306.7 nm was generated at a temperature-tuned AD^*A crystal by doubling the frequency of visible light at 613.4 nm, in a Spectra-Physics 380 ring-dye laser operating with Rhodamine R6G dye. The ring-dye laser was pumped by a 5 W Coherent Verdi cw laser operating at 532 nm. The absorption coefficient of the OH radical is well-established, and measured OH concentrations are accurate to better than ±5%.

The third wavelength at 227 nm was generated by quadrupling the frequency of the output from a Ti:Sapphire laser. HO_2 has a strong broadband absorption feature at deep UV wavelengths (210–250 nm) at temperatures ranging from room temperature to 1100 K [1–3,12]. The detection wavelength was chosen based on previous studies which suggest that the HO_2 absorption cross-section only weakly depends on temperature near this wavelength [2,3]. The Ti:Sapphire laser (MIRA HP, Coherent Inc.) was operated at a repetition rate of approximately 76 MHz (pulse

duration ~2 ps) between 700 and 980 nm with a peak output of 1 watt and a Gaussian spectral profile (FWHM ~ 1 nm). The near infrared output from the Ti:Sapphire laser was converted into UV light between 211 and 235 nm with a fourth harmonic generator (FHG, Coherent Inc.). Two silicon detectors with a bandwidth of 1 MHz (Newport 2032) were used to measure the intensities of both the reference beam (I_o) and the transmitted beam (I). The method has been previously used to investigate O_2 absorption cross-section at temperatures above 1100 K between 211 and 235 nm; details can be found in Ref. [13].

H_2O_2/Ar test mixtures were prepared following the procedure previously described [8,9]; key steps are outlined here. A polycarbonate flask that contained approximately 10 g of urea-H_2O_2 [$(NH_2)_2CO{\cdot}H_2O_2$] powder was placed in a 48 °C water bath. Urea-H_2O_2 gradually decomposed to yield H_2O_2 vapor, which was carried into the shock tube test section by a stream of research grade Ar (99.999%). To the knowledge of the authors, urea-H_2O_2 was first used as a reliable H_2O_2 source by Ludwig et al. [15]. A typical H_2O_2 concentration of about 2000 ppm can be achieved by setting argon flow rate to be 0.3–0.4 SLPM (standard liters per minute). A stable supply of H_2O_2 at this rate can be generated for approximately 3–4 h.

3. Analysis

It has been demonstrated in previous work [8,9] that initial H_2O_2 concentrations can be determined by taking the difference between the final and initial H_2O levels in a H_2O profile, as the overall conversion between H_2O and H_2O_2 is mole-for-mole. In addition, the curvature of H_2O time-histories is predominately controlled by the rate constant k_1 of reaction $H_2O_2 + M \rightarrow 2OH + M$ [9].

The combination of OH and H_2O time-histories provides sufficient information to determine the rate constant for $OH + H_2O_2 \rightarrow H_2O + HO_2$ (k_2) by accessing peak OH concentrations [8]. The rationale is that the OH concentration peaks soon after H_2O_2 decomposition is initiated, at which time species concentrations have the following order: $[HO_2] \ll [OH] \ll [H_2O_2]$. Therefore, the OH balance is determined predominately by Reactions (1) and (2).

In contrast, H_2O time-histories are not sensitive to, and reveal little information regarding, k_3 and k_4 [9]; and although the OH profiles are affected by Reactions (3) and (4), they do not, by themselves, place any strong modeling constraints on these rate constants individually. Additional information regarding the H_2O_2 reacting system becomes essential for accurate evaluation of k_3 and k_4. Theoretically, the determination of either HO_2 or H_2O_2 concentration automatically yields the value of the other species by the conservation of hydrogen atoms. In this study we have chosen to use an HO_2 diagnostic because of its stronger sensitivity to k_3 and k_4.

However, as briefly discussed in the introduction, due to the lack of high-fidelity ultraviolet HO_2 absorption cross-section data at relevant temperatures ($T > 1000$ K), laser absorption measurements at 227 nm only allow determination of relative shape of HO_2 time-histories. These HO_2 profile shapes provide information about the value of the ratios between k_3 and k_4, as will become evident in the following section. This information can be further used to infer absolute values of k_3 and k_4 by the addition of information from the OH time-histories, as Reactions (3) and (4) collectively affect OH concentrations. Once absolute values of k_3 and k_4 are determined, HO_2 absorption cross-sections at 227 nm can be calculated.

An iterative fitting approach was used in the analysis rather than a global fitting approach as a global approach would require somewhat arbitrary time-dependent weightings for each species time-history if the same level of sensitivity to each reaction rate constant is to be achieved. Because of this, we do not believe that a global fitting scheme would provide significantly improved final rate constants relative to the iterative approach.

4. Results and discussion

Shown in Fig. 1 are example H_2O and OH time-histories, which provide sufficient information to determine k_1 and k_2 values. Initial conditions in the post-reflected shock wave region were $T = 1182$ K, $P = 1.672$ atm. The composition of the initial test mixture was evaluated to

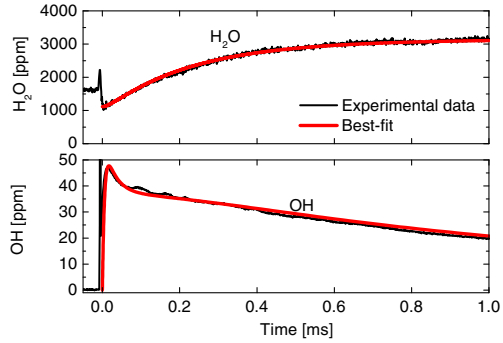

Fig. 1. From H_2O and OH time-histories, k_1 and k_2 were determined to be 1.44×10^8 cm^3 mol^{-1} s^{-1} and 5.88×10^{12} cm^3 mol^{-1} s^{-1}, respectively. The composition of the mixture is 2046 ppm H_2O_2/1113 ppm H_2O/556 ppm O_2/balance Ar. $T = 1182$ K, $P = 1.672$ atm.

be 2046 ppm H_2O_2/1113 ppm H_2O/556 ppm O_2/balance Ar using the H_2O diagnostic, where H_2O and O_2 were apparently formed from H_2O_2 wall decomposition prior to the arrival of the reflected shock wave, as detailed in our earlier studies [8,9]. It has been shown [9] that the presence of a trace amount of O_2 only has negligible effects on the kinetics of the H_2O_2 thermal decomposition system. The product of the initial O_2 concentration was estimated from the initial H_2O level by assuming stoichiometric H_2O_2 decomposition. For this example case, k_1 and k_2 were determined to be 1.44×10^8 cm^3 mol^{-1} s^{-1} and 5.88×10^{12} cm^3 mol^{-1} s^{-1}, respectively, where k_1 is defined as the second-order rate constant. Detailed procedures for inferring k_1 and k_2 have been reported in previous studies [8,9] and are omitted here. Estimated uncertainties in these k_1 and k_2 determinations are ±23% and ±17%, respectively.

To determine k_3 and k_4, the third diagnostic for HO_2 was introduced. An example laser absorbance time-history measured at 227 nm (radiation from the frequency-quadrupled Ti:Sapphire laser) over a pathlength of 15.2 cm behind a reflected shock wave is presented in Fig. 2, where the absorbance α was defined by the Beer–Lambert law as $\alpha = -\ln(I/I_o)$. The sample laser absorbance profile presents features that are common to all experimental data. Prior to the incident shock wave, a small level of laser absorbance was present due to H_2O_2 in the initial mixture, because H_2O_2 has a broad absorption spectrum overlapping with the entire HO_2 spectrum [2]. The mixture was heated to approximately 700 K by the incident shock wave, a temperature too low for any noticeable amount of H_2O_2 to decompose during the short period of time (~60 μs) before the arrival of the reflected shock wave.

The test mixture was then compressed by the reflected shock wave at time zero; a second jump

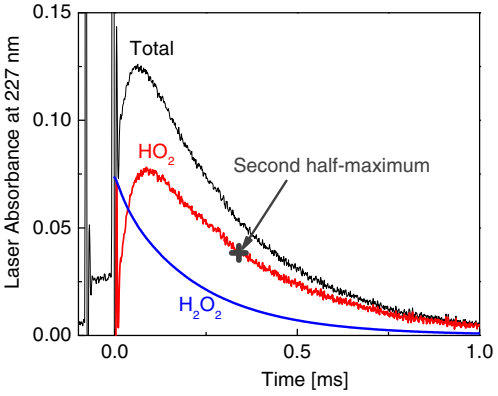

Fig. 2. Example time-history of laser absorbance at 227 nm over a pathlength of 15.2 cm. Conditions are those of Fig. 1.

in laser absorbance can be again attributed to increased H_2O_2 number density. Once the mixture was heated by the reflected shock wave, the rapid H_2O_2 decomposition reaction initiated. Two major factors contribute to the evolution of laser absorbance behind the reflected shock wave: the consumption of H_2O_2 and the growth and decline of HO_2. Laser absorption due to molecular oxygen is negligible (fractional absorption less than 10^{-4} at 227 nm at Fig. 1 conditions), despite the fact that the O_2 absorption cross-section is strongly temperature-dependent [13]. Total laser absorbance gradually approaches zero as the reaction progresses, confirming that there are no significant absorbing species other than H_2O_2 and HO_2.

Because H_2O_2 consumption is predominantly controlled by Reactions (1) and (2) [8,9], H_2O_2 concentration can be determined accurately using information obtained from OH and H_2O time-histories (see Fig. 1). Taking the laser absorbance level right after the reflected shock wave as a reference point, the laser absorbance time-history due to H_2O_2 can be calculated (blue curve in Fig. 2). The difference between the total laser absorbance profile and that due to H_2O_2 is the HO_2 absorbance time-history (red curve in Fig. 2). Note that the error in HO_2 absorbance inherited from the uncertainty in H_2O_2 concentration is negligible, because the H_2O_2 absorption cross-section is much smaller than that of HO_2 (approximately an order of magnitude smaller), as will be discussed later.

From HO_2 absorbance time-histories only relative shapes of HO_2 profiles can be reliably determined, because the absorption cross-section of HO_2 is subject to uncertainty. One key parameter to quantify the shape of HO_2 profiles is the time when HO_2 concentration decays back to half of its peak value, i.e., the second half-maximum (SHM) point, as denoted in Fig. 2. Similar to FHM points (first half-maximum) or peak points, SHM characterizes the net rates of HO_2 accumulation and consumption. Additionally, SHM provides much better time resolutions, because FHM and peak points are typically of much shorter time-scales than those of SHM points, due to the "skewed bell shapes" of HO_2 profiles (see Fig. 2).

In the example case presented in Fig. 2, SHM is observed at 0.34 ms. The dominant source of uncertainty in SHM is the uncertainty in H_2O_2 absorbance at time zero, as laser absorbance at time zero is shadowed by shock-induced Schlieren spikes at time zero. Uncertainty in SHM is estimated to be ±0.03 ms. With k_1 and k_2 pre-determined from H_2O and OH time-histories, SHM values can be calculated for a wide range of k_3–k_4 combinations at the conditions of Figs. 1 and 2, as presented in Fig. 3. The center line of the shadowed area corresponds to SHM = 0.34 ms;

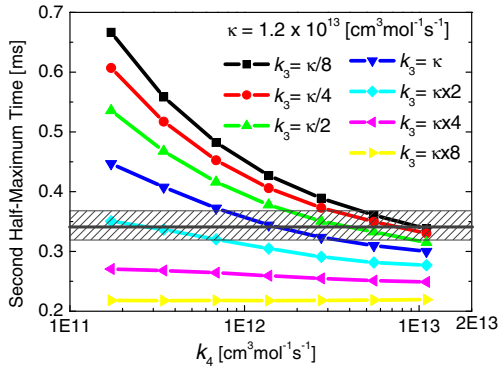

Fig. 3. Predicted second half-maximum (SHM) points of HO_2 profile at the conditions of Figs. 1 and 2. The shadowed area corresponds to SHM $= 0.34 \pm 0.03$ ms as determined from Fig. 2.

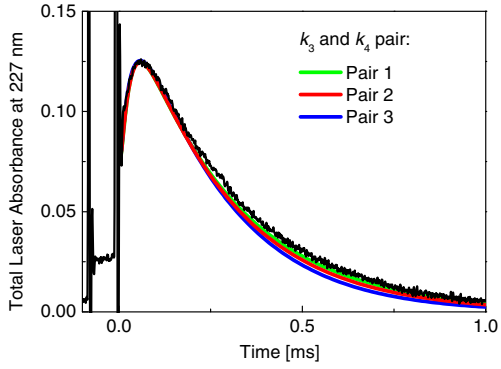

Fig. 4. The experimental laser absorbance at 227 nm can be well-fit by the predictions made with k_3 and k_4 pairs that give SHM = 0.34 ms. k_3–k_4 pairs are listed in Table 1. Test conditions are identical to those of Fig. 1.

whereas the boundaries of the band denote uncertainty limits.

As demonstrated in Fig. 4, the experimental laser absorbance at 227 nm can be well fitted by the predictions made with k_3–k_4 pairs (Table 1) that give SHM = 0.34 ms, where the HO_2 absorption cross-section was chosen for each k_3–k_4 pair by scaling the calculated HO_2 concentrations to match the peak absorbance. Species time-histories were calculated using a recent H_2/O_2 mechanism

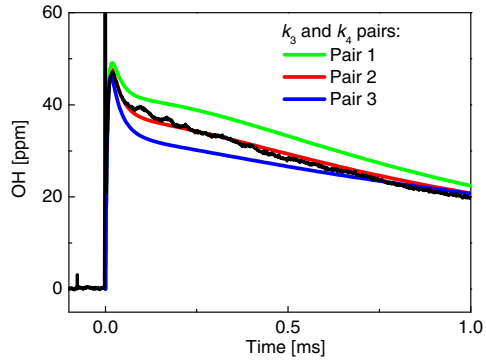

Fig. 5. The unique solution (pair 2) is selected from candidate k_3–k_4 pairs by analyzing the OH time-history. Test conditions are those of Fig. 1.

[14] as the base mechanism, with k_1–k_4 parameters updated to the ones dictated by current experimental data. It may be noted that the small laser absorbance prior to the incident shock wave was due to H_2O_2 vapor in the initial test mixture.

Although various k_3–k_4 combinations may give very similar shape in HO_2 profile, trends in k_3 and k_4 are opposite for a given SHM (see Fig. 3 and Table 1), which can be utilized to find a unique solution for k_3–k_4. In Table 1, notice that a 50% change in k_3 leads to less than a 10% difference in predicted peak HO_2 concentrations, as k_4 changes in the reverse direction and compensates for changes in HO_2 concentrations. With an approximately constant HO_2 level, higher k_3 values lead to smaller OH concentrations, because Reaction (3) ($OH + HO_2 \rightarrow H_2O + O_2$) directly removes OH radicals from the reacting system. The second pair of the k_3–k_4 combinations listed in Table 1 yields the best agreement with the experimental OH time-history, as demonstrated in Fig. 5. Therefore, k_3 and k_4 can be uniquely determined to be 1.5×10^{13} cm^3 mol^{-1} s^{-1} and 1.2×10^{12} cm^3 mol^{-1} s^{-1}, respectively. Note that k_2, the rate constant of Reaction (2) ($OH + H_2O_2 \rightarrow H_2O + HO_2$), was mainly inferred from OH concentrations at the peak [8]. Also note that a constant pressure reactor is assumed behind the reflected shock wave, as discussed in Ref. [8].

Uncertainty in k_3 and k_4 comes mainly from the fitting process. The uncertainty from determining SHM (shadowed area in Fig. 3) corresponds to

Table 1
k_3–k_4 pairs that yield SHM = 0.34 ms and the corresponding HO_2 absorption cross-sections that best-fit experimental data as shown in Fig. 2.

	k_3 [cm^3 mol^{-1} s^{-1}]	k_4 [cm^3 mol^{-1} s^{-1}]	$\sigma_{H_2O_2}$ [cm^2 mol^{-1}]	Peak HO_2 [ppm]	Best-fit σ_{HO_2} [cm^2 mol^{-1}]
Pair 1	1.0×10^{13}	1.6×10^{12}	1.4×10^5	242	1.17×10^6
Pair 2	1.5×10^{13}	1.2×10^{12}		231	1.27×10^6
Pair 3	2.2×10^{13}	0.8×10^{12}		210	1.41×10^6

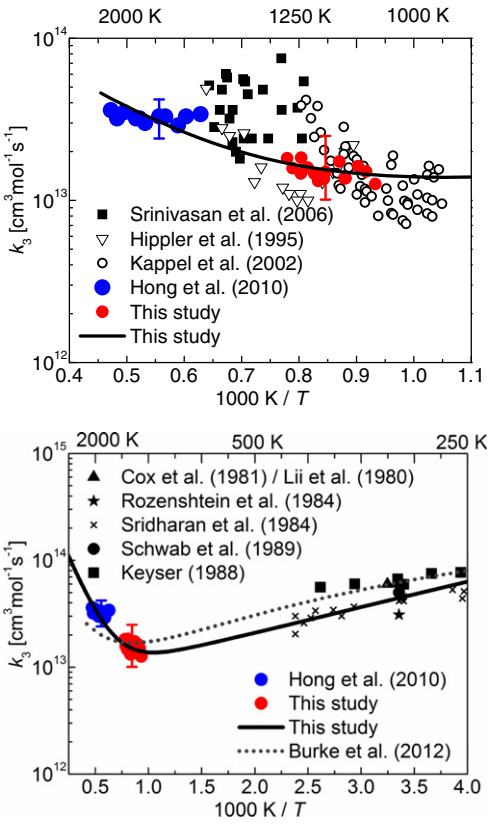

Fig. 6. Arrhenius plot of the rate constants of Reaction (3) ($OH + HO_2 \rightarrow H_2O + O_2$).

approximately a factor of 1.6 error in k_3 near $k_4 = 1.2 \times 10^{12}$ cm^3 mol^{-1} s^{-1}. In addition, the uncertainty in selecting the unique k_3–k_4 pair from fitting the OH time-history is estimated to be a factor of 1.3. Other uncertainty sources, such as temperature uncertainty, are minimized by using k_1 and k_2 parameters determined from experimental data of the same test. As discussed in previous work, the fitting uncertainty in k_1 and k_2 is on the order of 10% and can be neglected here. The overall fitting uncertainty in k_3 and k_4 is therefore estimated to be a factor of 1.67.

Tests were performed behind reflected shock waves at temperatures between 1072 and 1283 K, where the upper temperature limit was set by the need to determine the initial post-shock absorbance by H_2O_2 prior to reaction. As demonstrated in Fig. 2, the initial rise in laser absorbance at 227 nm becomes too rapid to be separated from the shock-induced Schlieren spikes at time zero if temperature is too high. Results for k_3 and k_4 are summarized in Arrhenius form in Fig. 6 and 7, respectively. Strong temperature dependency of the rate constant of Reaction (3) ($OH + HO_2 \rightarrow H_2O + O_2$) at temperatures near 1100 K has been reported in previous studies [4,5]. However, our

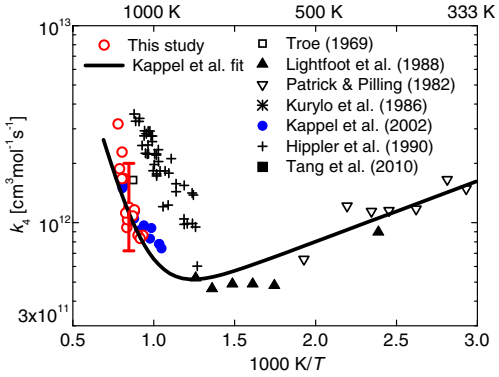

Fig. 7. Arrhenius plot of the rate constants of Reaction (4) ($HO_2 + HO_2 \rightarrow H_2O_2 + O_2$).

recent study suggests that k_3 does not have a strong temperature dependency at temperatures above 1600 K [6]. The lack of strong temperature dependency is supported by the current work, as evidenced by the upper panel of figure is 6. It worth noting that there is in fact relatively good agreement between the current work and Hippler et al. [4] and Kappel et al. [5] though there is larger scatter in the two earlier investigations. In addition, a recent theoretical study by Burke et al. [16,17] reported k_3 values that pass through the current work (Fig. 6).

A summation of two Arrhenius expressions can accurately represent the results of the current study, our previous one [6], as well as the studies at low temperatures [18–23]:

$$k_3 = 7.0 \times 10^{12} \exp(550/T) + 4.5 \times 10^{14} \times \exp(-5500/T)$$

and is shown as a solid black line in Fig. 6.

The rate constant of Reaction (4) ($HO_2 + HO_2 \rightarrow H_2O_2 + O_2$) has been the subject of many studies near room temperatures, for example, a study by Kurylo et al. [24] and a recent one by Tang et al. [25] between 253 and 323 K (and references therein). However, only a few studies have been reported at elevated temperatures: the study by Patrick and Pilling between 298 and 510 K [26], by Lightfoot et al. between 298 and 777 K [27], and studies near 1100 K [1,3,5]. Results of the current investigation are in good agreement with those reported in the literature [1,5], and therefore the expression recommended by Kappel et al. is kept unchanged:

$$k_4 = 1.0 \times 10^{14} \exp(-5556/T) + 1.9 \times 10^{11} \times \exp(709/T) \text{ [cm}^3 \text{ mol}^{-1} \text{ s}^{-1}\text{]}.$$

The absorption coefficients of H_2O_2 were determined behind both the incident and reflected

shock waves for each test following the procedure outlined earlier in this section. In the post-incident-shock region, the measured absorption cross-section of H_2O_2 at 227 nm can be represented by its mean value $\sigma_{H_2O_2}$ (683 K) = (1.1± 0.1) × 10^5 [cm^2/mol]. Similarly, the mean H_2O_2 absorption cross-section behind reflected shock waves is evaluated to be $\sigma_{H_2O_2}$ (1195 K) = (1.4± 0.1) × 10^5 [cm^2/mol] at the same wavelength. The mean absorption cross-section of HO_2 at 227 nm is estimated to be σ_{HO_2} (1195 K) = (13.1± 1.2) × 10^5 [cm^2/mol]. A dedicated study of H_2O_2 and HO_2 absorption cross-sections over a wide range of wavelengths in the vacuum-UV region is currently underway and will be reported in a future paper.

5. Conclusions

Given the importance of these hydrogen peroxide and hydroperoxy reactions in combustion kinetics, it is desirable to more fully characterize the H_2O_2 thermal decomposition system. Three laser absorption diagnostics, H_2O detection near 2.5 μm, OH at 306.7 nm, and HO_2 at 227 nm, were used simultaneously to study H_2O_2 thermal decomposition behind reflected shock waves. With H_2O and OH diagnostics, the rate constants for reactions $H_2O_2 + M \rightarrow 2OH + M$ (k_1) and $OH + H_2O_2 \rightarrow H_2O + HO_2$ (k_2) can be, and have been, reliably determined. With the addition of an HO_2 diagnostic at 227 nm, the important species involved in the H_2O_2 thermal decomposition reacting system have been measured for the first time in the temperature range covered by the current work. Specifically, the rate constants of reactions $OH + HO_2 \rightarrow H_2O + O_2$ (k_3) and $HO_2 + HO_2 \rightarrow H_2O_2 + O_2$ (k_4) can be inferred from the second half-maximum points (SHM) on HO_2 laser absorbance time-histories and OH concentrations.

A number of tests were performed at temperature between 1072 and 1283 K and at pressures near 1.7 atm. In contrast to the stronger temperature dependence reported in previous studies [4,5], a weaker temperature dependence for the rate constant of $OH + HO_2 \rightarrow H_2O + O_2$ was found in this work. The rate constants of reaction $HO_2 + HO_2 \rightarrow H_2O_2 + O_2$ determined in this work agree very well with those reported by Kappel et al. [5]; the recommendation therefore remains unchanged.

Acknowledgements

This material is based upon work supported by the National Science Foundation under Grant No. 0964884. The authors thank Dr. Burke at Argonne National Laboratory for sharing an unpublished manuscript with us.

Appendix A. Supplementary data

Supplementary data associated with this article can be found, in the online version, at http://dx.doi.org/10.1016/j.proci.2012.06.108.

References

[1] J. Troe, *Ber. Bunsen. Phys. Chem.* 73 (1969) 946–952.
[2] H. Kijewski, J. Troe, *Helv. Chim. Acta* 55 (1972) 205–213.
[3] H. Hippler, J. Troe, J. Willner, *J. Chem. Phys.* 93 (1990) 1755–1760.
[4] H. Hippler, H. Neunaber, J. Troe, *J. Chem. Phys.* 103 (1995) 3510–3516.
[5] Ch. Kappel, K. Luther, J. Troe, *Phys. Chem. Chem. Phys.* 4 (2002) 4392–4398.
[6] Z. Hong, S.S. Vasu, D.F. Davidson, R.K. Hanson, *J. Phys. Chem. A* 114 (2010) 5520–5525.
[7] N.K. Srinivasan, M.-C. Su, J.W. Sutherland, J.V. Michael, B. Ruscic, *J. Phys. Chem. A* 110 (2006) 6602–6607.
[8] Z. Hong, R.D. Cook, D.F. Davidson, R.K. Hanson, *J. Phys. Chem. A* 114 (2010) 5718–5727.
[9] Z. Hong, A. Farooq, E.A. Barbour, D.F. Davidson, R.K. Hanson, *J. Phys. Chem. A* 113 (2009) 12919–12925.
[10] R.K. Hanson, *Proc. Combust. Inst.* 33 (2011) 1–40.
[11] M.S. Wooldridge, R.K. Hanson, C.T. Bowman, *Int. J. Chem. Kinet.* 26 (1994) 389–401.
[12] P.D. Lightfoot, A.A. Jemi-Alade, *J. Photochem. Photobiol. A: Chem.* 59 (1991) l–10.
[13] Z. Hong, K.-Y. Lam, D.F. Davidson, R.K. Hanson, *J. Quant. Spectrosc. Radiat. Transfer* 112 (2011) 2698–2703.
[14] Z. Hong, D.F. Davidson, R.K. Hanson, *Combust. Flame* 158 (2011) 633–644.
[15] W. Ludwig, B. Brandt, G. Friedrichs, F. Temps, *J. Phys. Chem. A* 110 (2006) 3330–3337.
[16] M.P. Burke, S.J. Klippenstein, L.B. Harding, *Proceedings of the Combustion Institute,* this volume.
[17] M.P. Burke, Personal Communications.
[18] J.J. Schwab, W.H. Brune, J.G. Anderson, *J. Phys. Chem.* 93 (1989) 1030–1035.
[19] L.F. Keyser, *J. Phys. Chem.* 92 (1988) 1193–1200.
[20] U.C. Sridharan, L.X. Qiu, F. Kaufman, *J. Phys. Chem.* 88 (1984) 1281–1282.
[21] R.-R. Lii, R.A. Gorse Jr., M.C. Sauer Jr., S. Gordon, *J. Phys. Chem.* 84 (1980) 819–821.
[22] R.A. Cox, J.P. Burrows, T.J. Wallington, *Chem. Phys. Lett.* 84 (1981) 217–221.
[23] V.B. Rozenshtein, Yu.M. Gershenzon, S.D. Il'in, O.P. Kishkovitch, *Chem. Phys. Lett.* 112 (1984) 473–478.
[24] M.J. Kurylo, P.A. Ouellette, A.H. Laufer, *J. Phys. Chem.* 90 (1986) 437–440.
[25] Y. Tang, G.S. Tyndall, J.J. Orlando, *J. Phys. Chem. A* 114 (2010) 369–378.
[26] R. Patrick, M.J. Pilling, *Chem. Phys. Lett.* 91 (1982) 343–347.
[27] P.D. Lightfoot, B. Veyret, R. Lesclaux, *Chem. Phys. Lett.* 150 (1988) 120–126.